SCIENTIFIC REPORTS

OPEN

SUBJECT AREAS:
SENSORS
NANOSENSORS

Received
21 August 2013

Accepted
16 October 2013

Published
1 November 2013

Correspondence and requests for materials should be addressed to X.-J.H. (xingjiuhuang@iim.ac.cn)

A molecular-gap device for specific determination of mercury ions

Zheng Guo, Zhong-Gang Liu, Xian-Zhi Yao, Kai-Sheng Zhang, Xing Chen, Jin-Huai Liu & Xing-Jiu Huang

Nanomaterials and Environmental Detection Laboratory, Hefei Institutes of Physical Science, Chinese Academy of Sciences, Hefei 230031, P. R. China.

Specific determination/monitoring of trace mercury ions (Hg^{2+}) in environmental water is of significant importance for drinking safety. Complementarily to conventional inductively coupled plasma mass spectrometry and atomic emission/absorption spectroscopy, several methods, i.e., electrochemical, fluorescent, colorimetric, and surface enhanced Raman scattering approaches, have been developed recently. Despite great success, many inevitably encounter the interferences from other metal ions besides the complicated procedures and sophisticated equipments. Here we present a molecular-gap device for specific determination of trace Hg^{2+} in both standardized solutions and environmental samples based on conductivity-modulated glutathione dimer. Through a self-assembling technique, a thin film of glutathione monolayer capped Au nanoparticles is introduced into 2.5 μm-gap-electrodes, forming numerous double molecular layer gaps. Notably, the fabricated molecular-gap device shows a specific response toward Hg^{2+} with a low detection limit actually measured down to 1 nM. Theoretical calculations demonstrate that the specific sensing mechanism greatly depends on the electron transport ability of glutathione dimer bridged by heavy metal ions, which is determined by its frontier molecular orbital, not the binding energy.

Nanogap devices for electrical sensing have become a busy area of research which is continually expanding. The most intriguing feature of the devices is that they can directly transduce events of the molecules' specific binding into useful electrical signals, such as resistance/impedance, capacitance/dielectric, or field effect[1,2]. Of particular interest is the nanogapped gold particle film based on interdigital gold electrodes[3–11]. Some impressive works can be tracked back to studies conducted by Nagaoka, Murray and their colleagues. Nagaoka *et al.* demonstrated a molecular electronic device with an electrode spacing accuracy of a few nanometers (ca. 1.3 nm) by depositing dithiol-linked nanoparticles over the gap of the microelectrode. The sensing property was intimately involved in measuring the amount of nanoparticle building blocks of the nanogapped array on the microelectrode gap[12–16]. Murray *et al.* found that films of monolayer protected Au clusters with mixed alkanethiolate and ö-carboxylate alkanethiolate monolayers, linked together in a network polymer by carboxylate-Cu^{2+}-carboxylate bridges, exhibit electronic conductivities that vary with both the numbers of methylene segments in the ligands and the bathing medium (N_2, liquid or vapor)[17–20]. Very recently, we have demonstrated that such kind of nanogap device can be also designed as a streptvavidin biosensor[21]. By introducing β-cyclodextrin onto gold nanogapped electrodes' surfaces, it is further found that polychlorinated biphenyls can be detected based on specific inhibition of charge transport[22]. Despite these considerable progresses, a fundamental problem, the intrinsic electron transport feature of the nanogaps after being filled, still presents a significant experimental and theoretical challenge[23], which is very important for understanding the mechanism in sensing process.

As for one of the water pollutants, heavy metal ion, Hg^{2+}, has been receiving great attention because they are extremely harmful in the biosphere and even its trace amounts pose a detrimental risk to human health[24,25]. Therefore, sensitive and selective detection of this toxic metal ion is of significant importance in the environmental water. So far, various commonly used analytical methods, including cold-vapor atomic absorption spectroscopy, cold-vapor atomic fluorescence spectroscopy, inductively coupled plasma-mass spectrometry and inductively coupled plasma-atomic emission spectrometry, can be employed for sensitive, selective determination of Hg^{2+} [26–29]. However, these traditional central-laboratory measurements require expensive, sophisticated instruments, high operating costs and complicated sample-preparation processes, which are time consuming and unsuitable for routine in-field monitoring of a large number of samples. Also, samples may change during their collection, so efforts are ongoing to design rapid and inexpensive methods for the detection of Hg^{2+}. Currently, methods, such as colorimetry, fluorimetry and surface enhanced Raman scattering (SERS)[30–34], have been developed to allow miniaturization and field applications. Imperfectly, these still exhibit some features that limit their practical use, such as cross-sensitivity toward other metal ions and the sophistication needed to synthesize

probe materials. By comparison, electrochemical techniques are potentially most promising for determination of Hg^{2+} in the field, due to their high sensitivity and selectivity, rapid analysis time, impressive cost effectiveness and miniaturization[29,35–40], but they generally struggle with the ability of anti-interference.

Here we report a molecular-gap device by introducing glutathione (GSH) monolayer functionalized Au nanoparticles into a micro-gapped electrode and its application for electrical determination of toxic heavy metal ions. Although many other metal ions, such as Zn^{2+}, Cd^{2+}, Pb^{2+}, etc, could interact with a terminal carboxylic acid functional group of GSH, we find that such a molecular-gap device show an excellent specifity towards Hg^{2+}. The limit of detection (LOD) actually reaches about 1 nM. Theoretical calculations reveal that their frontier molecular orbitals of the formed glutathione dimer bridged by heavy metal ions between Au nanoparticles are responsible for the electron transfer of such a molecular-gap device.

Results

Fig. 1 briefly illustrates the experimental set-up for a molecular gap device. Firstly, as-synthesized Au nanoparticles (NPs) were functionalized with GSH monolayer. As Au NPs can interact with thiol groups through forming Au-S bonds on their surface, glutathione (GSH) with a thiol group (-SH) has been easily modified on the surface of Au NPs. It leads to the formation of Au@GSH nanoparticles, meaning that the surface of Au NPs is capped with a molecular layer of GSH and expose with carboxylic acid groups. Subsequently, Au@GSH NPs were self-assembled on SiO_2/Si substrate with an interdigital microelectrode, forming a sensing thin film consisted of numerous molecular-gaps. Accompanied with the introduction of heavy metal ions, these molecular-gaps were bridged by the complex formation of metal ions with two terminal carboxylic acid groups of GSH. Under a weak bias voltage, the current of the fabricated device is thus expected to be greatly changed. The sensing is based on conductivity-modulated glutathione dimer. That is, when the metal ions are trapped, the electron transport can be modulated in the transport channel. Thus, by monitoring the increase in current, it is possible to detect the specific binding of metal ions to terminal carboxylic groups of GSH.

Au NPs were prepared using a typical approach described elsewhere[41]. From its UV-visible absorbance spectrum, the adsorption peak is located at about 519.5 nm, indicating that the size of as-prepared Au NPs is about 20 nm (Supplementary Fig. S1a). It can be further demonstrated from a SEM image (Inset, Supplementary Fig. S1a). After being incubated in the aqueous solution containing GSH (0.025 mM) for 24 h, Au NPs were densely covered with GSH molecules. The formation of Au@GSH NPs (GSH modified Au NPs) is easily demonstrated by the appearance of specific bands in the infrared absorbance spectroscopy (Supplementary Fig. S1b). Some vibration peaks corresponding to specific groups of GSH, such as –NH, –COOH and –C=O, are clearly seen, even the emergence of the clear vibration peak of Au-S. It is concluded that the Au@GSH NPs is terminated with carboxylic acid groups. Moreover, XPS spectra also support that Au NPs are successfully decorated with GSH. We can observe that N and S elements from GSH molecules appear (Supplementary Fig. S1c). High-resolution XPS spectra (Supplementary Fig. S1d) indicate that N1s and S 2p peaks are centered at 400 and 161.8 eV, respectively.

Fig. 2a and b show high magnified TEM images of bare Au NPs and Au@GSH NPs, respectively. For bare Au NPs, evidently, their surfaces are smooth without any modifiers. After modification of GSH, the outer of Au NPs are covered with a thin layer marked by red dash lines, which is be ascribed to a few of GSH molecules non-specifically adsorbed their surface besides the GSH monolayer binding with Au NPs. Notably the thickness is about 1 ~ 2 nm, approximately equaling to the scale of a GSH molecular. Fig. 2c shows SEM image of Au@GSH NPs self-assembled between Au interdigital microelectrodes with the separated distance of 2.5 μm. It is seen that, with the complete evaporation of the solvent, Au@GSH NPs spread and closely packed together, the micro-gap electrodes are covered with a thin layer film consisted of numerous nanoparticles. From the magnified SEM image presented in Fig. 2d, these nanoparticles seem to be separated by numerous gaps with several nanometers. However, Au NPs are insulated by double molecular layers owing the existence of monolayer of GSH on their surfaces, which could be verified by the electrical measurements in the following part. These observations directly demonstrate the formation of molecular-gap between Au NPs through the monolayer of GSH on Au NPs surfaces. Additionally, it should be pointed out that, owing to the hydrophilicity of carboxylic groups of GSH exposed on the surface of Au NPs, poly(ethylene glycol) (PEG) dithiol is used to cross-link the Au NPs and stabilize the self-assembled film. From the optical photo shown in the inset of Fig. 2c, the fabricated device is portable, which is much smaller in comparison with a coin.

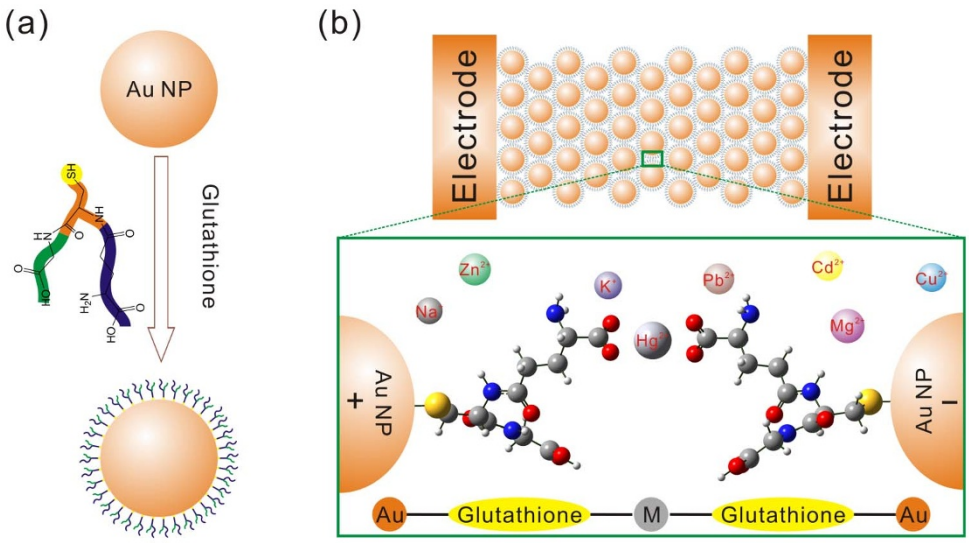

Figure 1 | Experimental set-up for molecular gap device. (a) Au NPs capped with glutathione monolayer; (b) Glutathione monolayer-capped Au NPs self-assembled between microelectrodes (top) and two glutathione molecules bridged via metal ions complexed with carboxylic groups between two Au NPs (bottom).

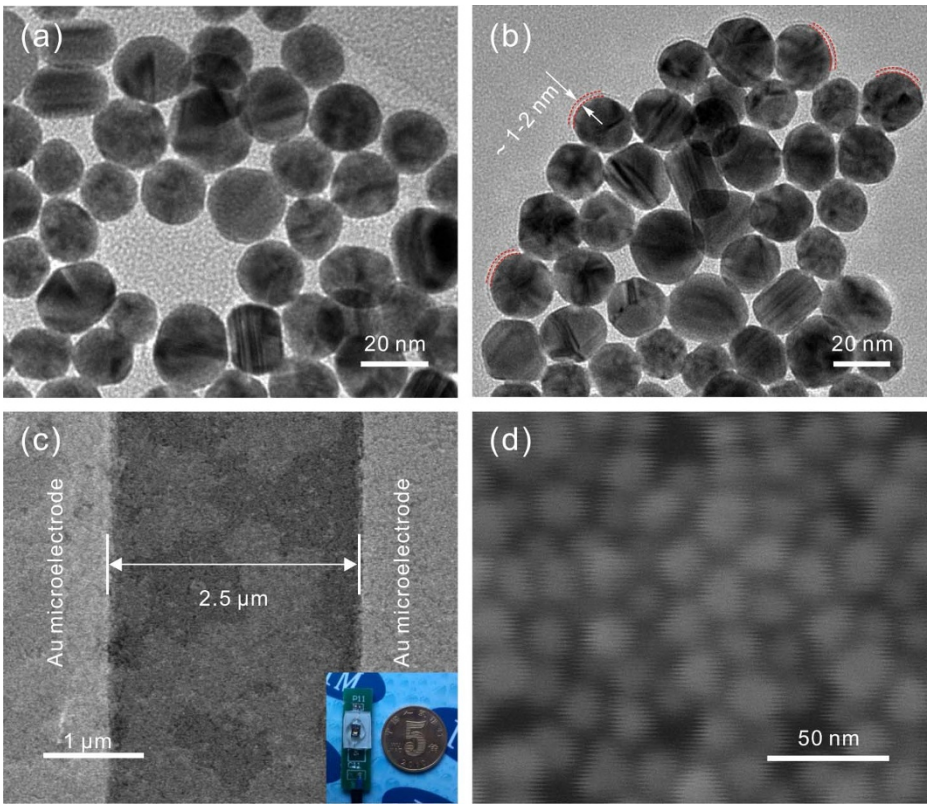

Figure 2 | Characterization. (a) High magnified TEM image of bare Au NPs. (b) High magnified TEM image of Au NPs capped with GSH (Au@GSH). 1–2 nm of GSH layer is clearly seen. (c) SEM image of two adjacent interdigital Au microelectrodes with self-assembled Au@GSH NPs, the inset corresponds to optical photo of the fabricated molecular-gap device. (d) Magnified SEM image of Au@GSH NPs between the interdigital Au microelectrodes.

Prior to the experiments of heavy metal ions sensing, the electrical characteristics of the fabricated molecular-gap devices have been firstly explored (Supplementary Fig. S2). As for the device assembled with Au NPs without any modifications, a good linearity is seen in I-V curve (Supplementary Fig. S2a). Obviously it still shows a good conductive property (the current is at level of mA), which is well agreement with previous reports[4]. However, the conductivity of the device assembled with Au@GSH NPs greatly deceases (the current is at a level of nA), which can be suggested the existence of molecule gap (Supplementary Fig. S2c). This result can be ascribed to double molecular layers of GSH, blocking the electron transport between Au NPs. For bare Au NPs, this "block effect" doesn't exist. Its resistance mainly arises from the impact contact of Au NPs with their neighboring nanoparticles. Scheme of their electron transport can be seen in Fig. S2b and d, respectively. Accordingly, the above electrical characterization indirectly proves the formation of a GSH molecular layer on the surface of Au NPs.

Since carboxylic acid group could interact with various metal ions[17], we wonder whether the conductivity of the Au@GSH NPs film consisted numerous molecular-gaps is changed. Firstly, Zn^{2+} and Hg^{2+} are employed as examples. I-V curves are recorded before and after binding with Zn^{2+} and Hg^{2+}, as shown in Fig. 3a and b, respectively. From Fig. 3a, after immersion in a 1 mM solution of Zn^{2+}, the slop of I-V curve (red line) does not evidently increase in contrast to the black line of blank, implying that the conductance of the films is virtually unchanged. However, when being immersed into a 1 mM solution of Hg^{2+}, it can be clearly observed that its conductivity is remarkably increased, inferring from the I-V curve (green line) shown in Fig. 3b. Enlightened by the above results, such a molecular-gap device could be potentially used to the detection of Hg^{2+}. Under a certain bias voltage, the real-time response curve toward different concentration of Hg^{2+} has been performed, as depicted in Fig. 3c. From the inset, obvious sensing signal can be seen when the concentration of Hg^{2+} is down to 1 nM, indicating that the fabricated molecular-gap device with a very low detection limit actually measured. Relative to the blank, the flowing current gradually increases with the incensement of its concentration. Up to 0.1 mM, it is greatly changed. In order to demonstrate the positive sensing characteristics arised from GSH molecules, another film assembled with bare Au NPs linked with PEG dithiol has further been investigated. Different from the film consisted of bare Au NPs, its resistivity is very larger similar with that of Au@GSH NPs. The reason can be attributed that Au NPs is partly insulted by PEG dithiol molecules to some extent. The real-time sensing curve toward different concentration of Hg^{2+} is shown in Fig. S3 (Supplementary). Clearly, no response has been observed when the concentration is lower than 1 μM. Further increasing to 1 mM, a weak response can be seen. However, it can be neglected, compared with that of Au@GSH NPs film. It is suggested that the monolayer of GHS is very critical for the sensing properties of the fabricated molecular-gap device. Besides Hg^{2+} and Zn^{2+}, other metal ions have also been explored carefully (Supplementary Fig. S4). We find that the responses of the molecular-gap device toward all investigated metal ions are not evident except for Hg^{2+}. Even at their high concentration of 1 mM, it still shows no response. Based on the comparison of the sensitivity shown in Fig. 3d, it can be concluded that the fabricated molecular-gap device exhibits a specific selectivity toward metal ions and can be effectively employed for the determination of Hg^{2+} in the real water sample without any interferences from other metal ions.

To illuminate the specific sensing mechanism of such a molecular-gap device, theoretical calculations have been further performed. Generally, the selectivity of sensing devices mainly depends on the formation of complex between the analyte and sensing materials. In the following, the interaction between the carboxylic acid groups of

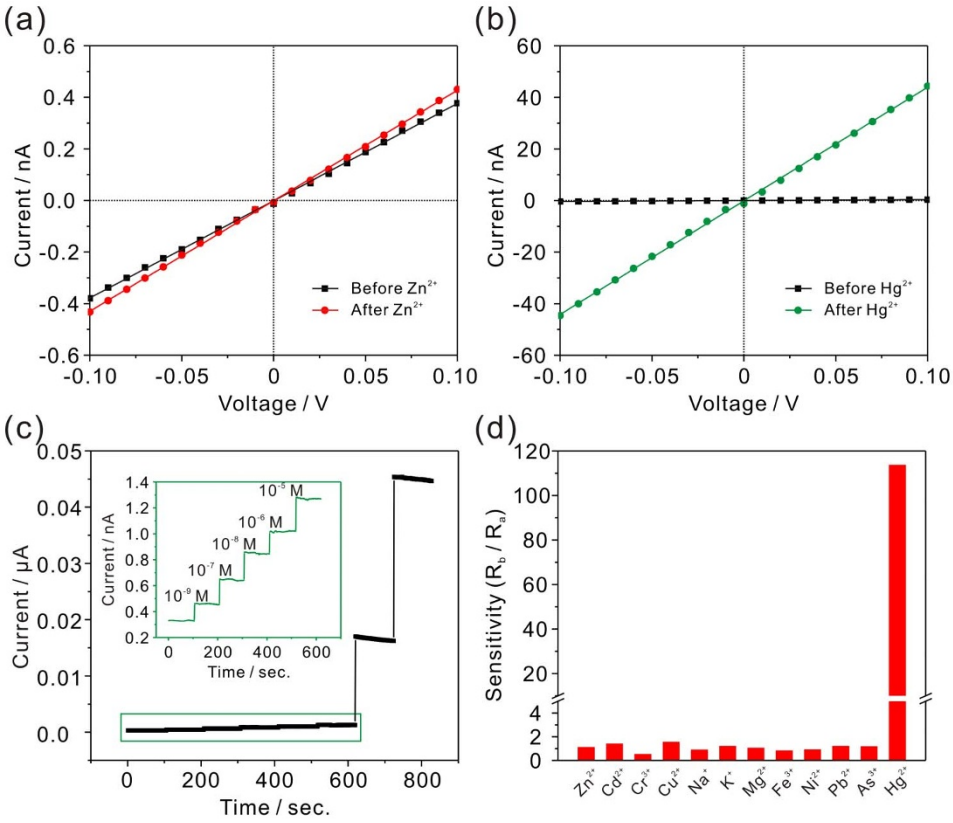

Figure 3 | Typical I-V plots and sensitivity and specifity toward Hg^{2+} by fabricated molecular gap device. (a–b) I-V curves for molecular gap devices before and after exposure to Zn^{2+} (1 mM) and Hg^{2+} (1 mM), respectively. The conductance is virtually unchanged after immersion in 1 mM solution of Zn^{2+}, and results in a marked change in a 1 mM solution of Hg^{2+}. (c) Real-time sensing curve under different concentration of Hg^{2+} for the molecular-gap device under a bias voltage of 0.1 V. (d) Specifity of the fabricated molecular-gap device. The concentration of all investigated metal ions is 1 mM; R_b and R_a are the resistance of the device before and after immersion, respectively.

glutathiose part for GSH and metal ions (Zn^{2+}, Cd^{2+}, Hg^{2+} and Pb^{2+} as examples) have been representatively selected to perform the theoretical calculations. Before binding with metal ions, GSH among Au nanoparticles forms a dimer with hydrogen bonding. After being incubated into the solution containing metal ions, terminal carboxylic acid groups of GSH are linked with metal ions, leading to the formation of a complex between two GSH molecules. All optimized geometries and binding energy are shown in Fig. S5 and Table S1 (Supplementary), respectively. Based on the binding energy, it can be found that GSH easily binds with the investigated heavy metal ions such as Zn^{2+}, Cd^{2+}, Hg^{2+} and Pb^{2+}. Furthermore, their binding energy follows the turn of $Zn^{2+} > Cd^{2+} \approx Hg^{2+} > Pb^{2+}$, which is not consistent with the selectivity of the molecular-gap device to Hg^{2+}. It means that GSH binding with metal ions is only necessary to realize the conductivity change of molecular-gap device, not sufficient. Furthermore, As^{3+} has also been explored. Concerning to colorimetric selective detection of As^{3+} by GSH modified Au NPs, Ray et al. reported that each As^{3+} can bind with three GSH molecules via an As-O linkage, leading to the aggregation of Au NPs[42]. In fact, As^{3+} exists with $As(OH)_3$ in neutral solution. Here, similar with GSH binding with Zn^{2+}, Cd^{2+}, Hg^{2+} and Pb^{2+}, two GSH molecules have been employed to complex with $As(OH)_3$, leading to the loss of two H_2O molecules (Optimized geometry seen in the supplementary information). However, the calculated results indicate that the above process is endothermic reaction, implying that it is less favorable for GSH binding with As^{3+} in thermodynamics in contrast to other metal ions.

According to previous reports about the electron transport of molecular junction, the conductivity of molecular mainly depends on its frontier orbital[23,43–46]. Initiate from this view, frontier orbital of GSH dimer and its complexes with metal ions have been further investigated. The energies of their highest occupied molecular orbital (HOMO) and lowest unoccupied molecular orbital (LUMO) are listed in Table S2 (More details can be seen in the Supplementary Information). The energy gap between of them is described in Fig. 4a. For the GSH dimer, its energy gap is about 6.17 eV. Once combined with metal ions, their energy gaps are changed. Bridged by Zn^{2+}, it deceases to 5.76 eV. Similar effects can be seen with the binding of Cd^{2+}, Hg^{2+} and Pb^{2+}. It is about 4.89 eV for Cd^{2+} and 3.86 eV for Hg^{2+}, indicating that the energy gap gradually decreases from top to bottom along the same group. However, linked by Pb^{2+}, it is about 5.29 eV larger than that of the complex bridged by the same periodic Hg^{2+}. From the Fig. 4b, it can be found that the HOMO orbitals are always located, which is closed to the connected Au NPs for GSH dimer before and after binding with heavy metal ions. For the LUMO orbital, it is mostly centered and separated at the centre of its dimer before binding. However, after binding it mainly focused on metal atoms. To realize the electron flowing between two Au NPs, the electrons should be injected from the HOMO into the LUMO. Combined with the analysis of HOMO and LUMO for GSH dimer and their complexes, possible specific sensing mechanism has been offered in the following. The electron transport process is illustrated in Fig. 5, which shows an idealized band diagram. The energy (E_a) at which the majority of tunneling occurs is above the Fermi energy (E_f) but below the LUMO. Under a given applied bias voltage, the electron transport between Au NPs mainly depends on the thermally assisted tunneling effect for the model *a*, in which the LUMO (−0.41 eV) of GSH dimer between Au NPs will be higher than E_a

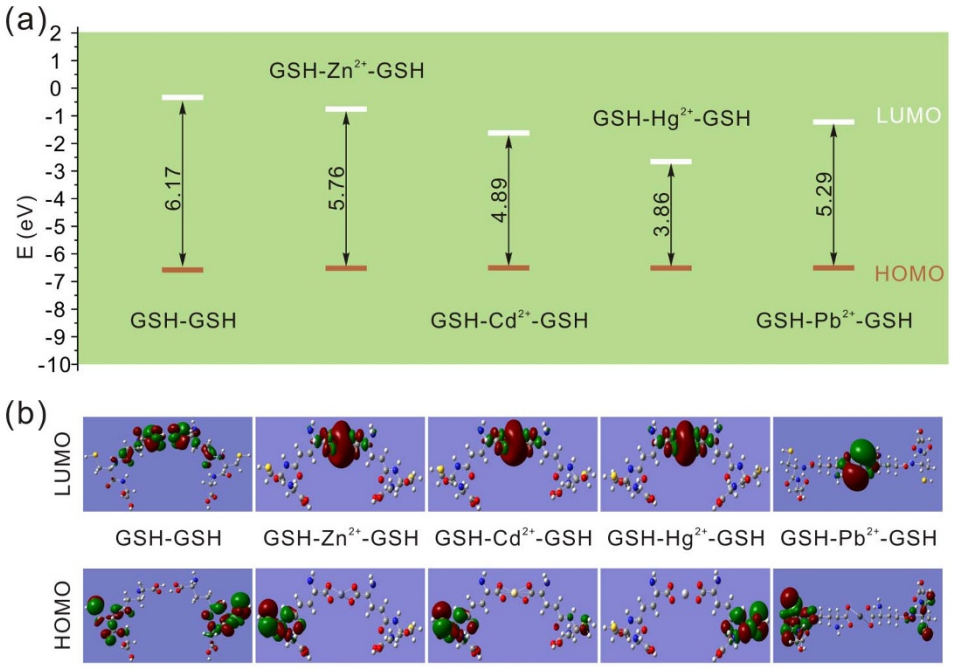

Figure 4 | Comparative studies of the energies of the molecular orbitals of the complexes. (a) HOMO and LUMO energy gap of GSH dimer and complexes of GSH dimer bridged by Zn^{2+}, Cd^{2+}, Hg^{2+} and Pb^{2+}. (b) HOMO and LUMO. The case before capture of cations (marked by GSH-GSH) was included for comparison.

without binding with metal ions. After binding with Zn^{2+}, Cd^{2+} and Pb^{2+}, their energies of LUMO are decreased to −0.76, −1.62 and −1.22 eV, respectively. Maybe they are still higher than E_a, as shown in the model *b*. However, for Hg^{2+} it is down to −2.65 eV, which may be close or lower than E_a. Furthermore, the energy gap of HOMO and LUMO is down to 3.86 eV, which is greatly lower than those of GSH dimer binding with other metal ions. Accordingly, electrons should be easily injected from the HOMO into the LUMO, leading to the enhancement of electron transport in the model *c*.

Discussion

Compared with previous works on the detection of mercury ions using typical electrochemical, fluorescent, colorimetric and surface enhanced Raman scattering (SERS) methods[30–37], the fabricated molecular-gap device realizes a specific sensing performance with a detection limit actually measured down to 1 nM and will not be interfered by other metal ions even at a high concentration (1 mM). Hence it can be used to determine mercury ions in the complicated background of real water sample without any chemical pretreatments. Additionally, its repeatability has also been demonstrated through independently fabricating many devices with a good sensing performance toward Hg^{2+}. However, owing to a strong affinity of Hg^{2+} with carboxylic acid groups of GSH, the reusability of the fabricated device is limited. Accordingly, to realize its reusability, it is a possible route to employ other organic ligands with a stronger affinity to displace Hg^{2+} from GSH. Further work is undergoing. Theoretical calculations indicate that the sensing performance does not correlate with the calculated binding energies of metal ions with glutathione dimer, only depend on the ΔE of their HOMO/LUMO gap, which is involved in electron transport. Based on the inherent characteristics of electron transport for the complex between GSH dimer and metal ions, specific sensing to mercury ions from environmental water is possible, indicating the high potential of this methodology in environmental monitoring and various chemical sensing.

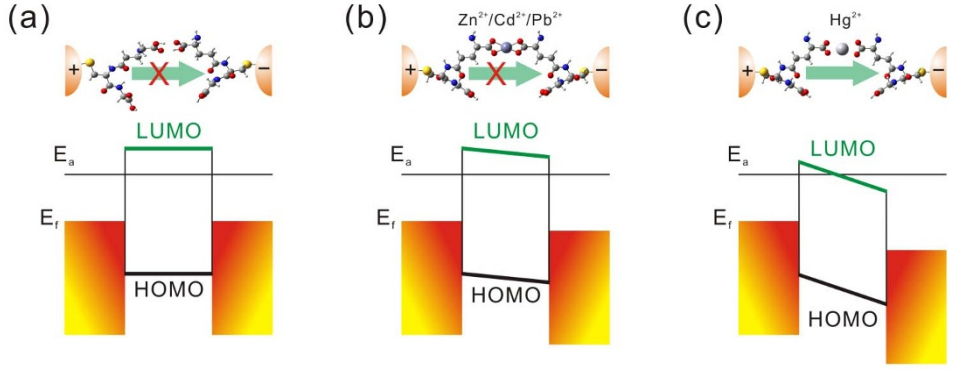

Figure 5 | Idealized band diagram for fabricated molecular-gap device linked with cations including Hg^{2+}. (a) The flat band condition, where E_f is the Fermi energy of the Au NPs in relation to the HOMO-LUMO levels of the complex; E_a is the energy at some level above the Fermi level in which thermally assisted tunneling occurs. (b–c) The cases for varies of cations with an applied voltage across the junction. Panels *a* and *b* show that the charge transport can be inhibited.

In conclusion, a molecular-gap device has been demonstrated through assembling with Au@GSH NPs between interdigital microelectrodes. Based on the special structure of GSH, the fabricated nanodevice shows a specific response towards Hg^{2+}. The lowest detectable concentration actually measured is 1 nM. Theoretical calculations reveal that the conductance between Au nanoparticles isolated by GSH does not correlate with the charge of metal ions and the calculated binding energy of the complexation of the cations by Au@GSH NPs. It greatly depends on the energy gap between LUMO and HOMO for the complex, which forms via a bridge connection between metal ion and carboxylic groups of two GSHs. This finding will expectedly mark a new route to develop future environmental sensors with the sensing specificity. With further striving, it should be possible to extend the applicability for the present molecular-gap devices to other sensing systems whose properties derive from molecular specific recognition on NP surfaces in a solid state.

Methods

Preparation of glutathione monolayer capped Au nanoparticles. Au nanoparticles were synthesized following Fren's method[41]. Briefly, the mixture solution of 99 ml H_2O and 1 ml $HAuCl_4$ (1%) is uniform under stirring, then heated to be boiling. Afterwards, 6 ml trisodium citrate (1%) was added immediately. After 30 min under refluxing and naturally cooled to room temperature, the solution containing Au nanoparticles was obtained. In order to functionalize Au nanoparticles, glutathione (0.025 mM) was added into the above solution with stirring for 1 h and subsequently immobilized for 24 h without disturbance. Then Au nanoparticles are capped with monolayer of glutathione.

Fabrication of molecular-gap devices and sensing measurements. In order to fabricate the molecular-gap device, GSH monolayer-capped Au nanoparticles were self-assembled on the interdigital Au microelectrodes with 2.5 μm of the separated distance, which was constructed using electron beam lithography on Si wafer with a 1 μm coating of SiO_2. With the complete evaporation of solvents, GSH monolayer functionalized Au nanoparticles were closely packed together, forming a thin layer film. Owing to the hydrophilicity of carboxylic groups exposed on the Au nanoparticles, as-fabricated thin film is not stable. To prevent its re-dissolution on exposure to solvent, the film was reinforced by cross-linking the Au nanoparticles with PEG dithiol. Subsequently, the film was washed with an excess of ethanol and water, dried under a stream of N_2. Then, in order to assure the stability of the fabricated device during the working process, it was fixed on a small PC board and sealed with AB glue exposing with the working area.

A Keithley 6487 picoameter/voltage sourcemeter was employed to serve as both voltage source and current reader. The fabricated devices were subsequently immersed in the solutions of metal ions with concentrations ranging from 1 nM to 1 mM. The mercury detection experiment was performed by diluting Hg^{2+} ($Hg(NO_3)_2$ Sigma Aldrich). Actually fraction of the Hg^{2+} ions with respect to the other components ($Hg(NO_3)_2$, $(HgNO_3)^+$ and its hydrolytic species) in aqueous solution varies depending on the ionization equilibrium[47], which was neglected in this case. Similar process has also been employed to prepare the solution of other metal ions. After immersion, the devices were washed with amounts of water to remove excess salt and were then completely dried under a flow of nitrogen. All subsequent electrical measurements and sensing performances were performed in a closed glass chamber at room temperature under dry air.

Characterization. The scanning electron microscopy SEM images were taken by a FEI Quanta 200 FEG field emission scanning electron microscope. The TEM and HRTEM images analyses were carried out on a JEM-2010 microscope. The infrared (IR) spectra were obtained with a Nicolet Nexus-670 FT-IR spectrometer. X-Ray photoelectron spectroscopy (XPS) analyses of the samples were conducted on a VG ESCALAB MKII spectrometer using an Mg Kα X-ray source (1253.6 eV, 120 W) at a constant analyzer. The energy scale was internally calibrated by referencing the binding energy (E_b) of the C 1s peak at 284.60 eV for contaminated carbon. Furthermore, UV–visible absorbance spectrum was also measured with a UNIC UV-4802 spectrometer.

Theoretical calculations. To illuminate the specific sensing mechanism at the level of molecular understanding, theoretical calculations were performed with the Gaussian 03 software package[48]. The hybrid density functional method, including Beck's three parameters nonlocal–exchange functional with the correlation functional of Lee–Yang–Parr (B3LYP)[49,50], was employed with LANL2DZ[51–53] pseudopotential for metal atoms and a standard all–electron split–valence basis set 6–31G* for other atoms (C, H, N, O and S). All molecular geometry optimization were carried without geometry or symmetry constraints. The minima at potential energy surface corresponding to each structure have been assured by performing calculations on vibrational frequencies. The values of binding energy, ΔE, indicated the stability of two GSH molecules bridged by a metal ion. For systems under consideration, it is defined as the following equation: $\Delta E = E_{Complex} - (2E_{GSH} + E_M)$, where $E_{Complex}$ is the energy of complexes, E_{GSH} is the energy of GSH anion corresponding to the removal of hydrogen of carboxylic group for its glutathiose part, and E_M is the energy of metal ions. The energies reported have been corrected by inclusion of zero-point energies (ZPE), unless otherwise specified explicitly.

1. Chen, X. *et al*. Electrical nanogap devices for biosensing. *Mater. Today* **13**, 28–41 (2010).
2. Albrecht, T. Electrochemical tunnelling sensors and their potential applications. *Nat. Commun.* **3**, 1–8 (2012).
3. Lai, L. M. H. *et al*. The biochemiresistor: An ultrasensitive biosensor for small organic molecules. *Angew. Chem. Int. Ed.* **51**, 6456–6459 (2012).
4. Morag, A. *et al*. Self-assembled transparent conductive electrodes from au nanoparticles in surfactant monolayer templates. *Adv. Mater.* **23**, 4327–4331 (2011).
5. Garcia-Berrios, E. *et al*. Response versus chain length of alkanethiol-capped au nanoparticle chemiresistive chemical vapor sensors. *J. Phys. Chem. C* **114**, 21914–21920 (2010).
6. Snow, A. W., Ancona, M. G. & Park, D. Nanodimensionally driven analyte response reversal in gold nanocluster chemiresistor sensing. *Langmuir* **28**, 15438–15443 (2012).
7. Yin, J. *et al*. Molecularly mediated thin film assembly of nanoparticles on flexible devices: electrical conductivity versus device strains in different gas/vapor environment. *ACS Nano* **5**, 6516–6526 (2011).
8. Wang, L. Y. *et al*. Flexible chemiresistor sensors: thin film assemblies of nanoparticles on a polyethylene terephthalate substrate. *J. Mater. Chem.* **20**, 907–915 (2010).
9. Wohltjen, H. & Snow, A. W. Colloidal metal-insulator-metal ensemble chemiresistor sensor. *Anal. Chem.* **70**, 2856–2859 (1998).
10. Ibanez, F. J. & Zamborini, F. P. Chemiresistive sensing with chemically modified metal and alloy nanoparticles. *Small* **8**, 174–202 (2012).
11. Ikeda, M., Tanifuji, N., Yamaguchi, H., Irie, M. & Matsuda, K. Photoswitching of conductance of diarylethene-Au nanoparticle network. *Chem. Commun.* 1355–1357; DOI: 10.1039/B617246F (2007).
12. Tokonami, S., Shiigi, H. & Nagaoka, T. Open bridge-structured gold nanoparticle array for label-free DNA detection. *Anal. Chem.* **80**, 8071–8075 (2008).
13. Shiigi, H., Tokonami, S., Yakabe, H. & Nagaoka, T. Label-free electronic detection of DNA-hybridization on nanogapped gold particle film. *J. Am. Chem. Soc.* **127**, 3280–3281 (2005).
14. Shiigi, H., Yamamoto, Y., Yakabe, H., Tokonami, S. & Nagaoka, T. Electroical property and water repellency of a networked monolayer film prepared from Au nanoparticles. *Chem. Commun.* 1038–1039; DOI: 10.1039/B212226J (2003).
15. Tokonami, S., Shiigi, H. & Nagaoka, T. Characterization and DNA sensing properties of nanogapped array electrodes. *J. Electrochem. Soc.* **155**, J105–J109 (2008).
16. Tokonami, S., Shiigi, H. & Nagaoka, T. Preparation of nanogapped gold nanoparticle array for DNA detection. *Electroanalysis* **20**, 355–360 (2008).
17. Zamborini, F. P., Hicks, J. F. & Murray, R. W. Quantized double layer charging of nanoparticle films assembled using carboxylate/(Cu^{2+} or Zn^{2+})/carboxylate bridges. *J. Am. Chem. Soc.* **122**, 4514–4515 (2000).
18. Zamborini, F. P. *et al*. Electron hopping conductivity and vapor sensing properties of flexible network polymer films of metal nanoparticles. *J. Am. Chem. Soc.* **124**, 8958–8964 (2002).
19. Wuelfing, W. P., Green, S. J., Pietron, J. J., Cliffel, D. E. & Murray, R. W. Electronic conductivity of solid-state, mixed-valent, monolayer-protected Au clusters. *J. Am. Chem. Soc.* **122**, 11465–11472 (2000).
20. Chen, S. W. *et al*. Gold nanoelectrodes of varied size: Transition to molecule-like charging. *Science* **280**, 2098–2101 (1998).
21. Yu, Y. *et al*. CdSe Quantum dots enhance electrical and electrochemical signals of nanogap devices for bioanalysis. *Small* **8**, 3274–3281 (2012).
22. Yu, Y., Chen, X., Wei, Y., Liu, J. H. & Huang, X. J. Strategy for polychlorinated biphenyl detection based on specific inhibition of charge transport using a nanogapped gold particle film. *Anal. Chem.* **84**, 9818–9824 (2012).
23. Ratner, M. A brief history of molecular electronics. *Nat. Nanotechnol.* **8**, 378–381 (2013).
24. Tchounwou, P. B., Ayensu, W. K., Ninashvili, N. & Sutton, D. Environmental exposure to mercury and its toxicopathologic implications for public health. *Environ. Toxicol.* **18**, 149–175 (2003).
25. Leermakers, M., Baeyens, W., Quevauviller, P. & Horvat, M. Mercury in environmental samples: Speciation, artifacts and validation. *TrAC-Trend. Anal. Chem.* **24**, 383–393 (2005).
26. Nixon, D. E., Burritt, M. F. & Moyer, T. P. The determination of mercury in whole blood and urine by inductively coupled plasma mass spectrometry. *Spectrochim. Acta B* **54**, 1141–1153 (1999).
27. Fong, B. M. W., Siu, T. S., Lee, J. S. K. & Tam, S. Determination of mercury in whole blood and urine by inductively coupled plasma mass spectrometry. *J. Anal. Toxicol.* **31**, 281–287 (2007).
28. Fernandez, C., Conceicao, A. C. L., Rial-Otero, R., Vaz, C. & Capelo, J. L. Sequential flow injection analysis system on-line coupled to high intensity focused ultrasound: Green methodology for trace analysis applications as demonstrated for the determination of inorganic and total mercury in waters and urine by cold vapor atomic absorption spectrometry. *Anal. Chem.* **78**, 2494–2499 (2006).

29. Gao, C. & Huang, X. J. Voltammetric determination of mercury(II). *TrAC-Trend. Anal. Chem.* **51**, 1–12 (2013).
30. Gu, Z., Zhao, M. X., Sheng, Y. W., Bentolila, L. A. & Tang, Y. Detection of mercury ion by infrared fluorescent protein and its hydrogel-based paper Assay. *Anal. Chem.* **83**, 2324–2329 (2011).
31. Huang, C. C., Yang, Z., Lee, K. H. & Chang, H. T. Synthesis of highly fluorescent gold nanoparticles for sensing Mercury(II). *Angew. Chem. Int. Ed.* **46**, 6824–6828 (2007).
32. Coronado, E. *et al*. Reversible colorimetric probes for mercury sensing. *J. Am. Chem. Soc.* **127**, 12351–12356 (2005).
33. Lee, J. S., Han, M. S. & Mirkin, C. A. Colorimetric detection of mercuric ion (Hg^{2+}) in aqueous media using DNA-functionalized gold nanoparticles. *Angew. Chem. Int. Ed.* **46**, 4093–4096 (2007).
34. Senapati, T. *et al.* Highly selective SERS probe for Hg(II) detection using tryptophan-protected popcorn shaped gold nanoparticles. *Chem. Commun.* **47**, 10326–10328 (2011).
35. Zhu, Z. Q. *et al.* Highly sensitive electrochemical sensor for mercury(II) ions by using a mercury-specific oligonucleotide probe and gold nanoparticle-based Amplification. *Anal. Chem.* **81**, 7660–7666 (2009).
36. Zhao, Z. Q., Chen, X., Yang, Q., Liu, J. H. & Huang, X. J. Beyond the selective adsorption of polypyrrole-reduced graphene oxide nanocomposite toward Hg^{2+}: Ultra-sensitive and -selective sensing Pb^{2+} by stripping voltammetry. *Electrochem. Commun.* **23**, 21–24 (2012).
37. Zhao, Z. Q., Chen, X., Yang, Q., Liu, J. H. & Huang, X. J. Selective adsorption toward toxic metal ions results in selective response: electrochemical studies on a polypyrrole/reduced graphene oxide nanocomposite. *Chem. Commun.* **48**, 2180–2182 (2012).
38. Fu, X. C. *et al.* Three-dimensional gold micro-/nanopore arrays containing 2-mercaptobenzothiazole molecular adapters allow sensitive and selective stripping voltammetric determination of trace mercury (II). *Electrochim. Acta* **56**, 463–469 (2010).
39. Fu, X. C. *et al.* Stripping voltammetric detection of mercury(II) based on a surface ion imprinting strategy in electropolymerized microporous poly(2-mercaptobenzothiazole) films modified glassy carbon electrode. *Anal. Chim. Acta* **685**, 21–28 (2011).
40. Fu, X. C. *et al.* Electropolymerized surface ion imprinting films on a gold nanoparticles/single-wall carbon nanotube nanohybrids modified glassy carbon electrode for electrochemical detection of trace mercury(II) in water. *Anal. Chim. Acta* **720**, 29–37 (2012).
41. Brown, K. R., Walter, D. G. & Natan, M. J. Seeding of colloidal Au nanoparticle solutions. 2. Improved control of particle size and shape. *Chem. Mater.* **12**, 306–313 (2000).
42. Kalluri, J. R. *et al.* Use of gold nanoparticles in a simple colorimetric and ultrasensitive dynamic light scattering assay: Selective detection of arsenic in groundwater. *Angew. Chem. In. Ed.* **48**, 9668–9671 (2009).
43. Vazquez, H. *et al.* Probing the conductance superposition law in single-molecule circuits with parallel paths. *Nat. Nanotechnol.* **7**, 663–667 (2012).
44. Guedon, C. M. *et al*. Observation of quantum interference in molecular charge transport. *Nat. Nanotechnol.* **7**, 304–308 (2012).
45. Das, B. Modeling selective single molecule sensors for transition metal ions. *J. Phys. Chem. C* **113**, 16203–16209 (2009).
46. Zhang, Z. H. *et al.* A dramatic odd-even oscillating behavior for the current rectification and negative differential resistance in carbon-chain-modified donor-acceptor molecular devices. *Adv. Funct. Mater.* **23**, 2765–2774 (2013).
47. Hoang, C. V., Oyama, M., Saito, O., Aono, M. & Nagao, T. Monitoring the presence of ionic mercury in environmental water by plasmon-enhanced infrared spectroscopy. *Sci. Rep.* **3**, 1175; DOI: 10.1038/srep01175 (2013).
48. Frisch, M. J. *et al*. Gaussian 03, Revision E.01, Gaussian, Inc.: Wallingford, CT. (2004).
49. Becke, A. D. Density-functional thermochemistry 3. The role of exact exchange. *J. Chem. Phys.* **98**, 5648–5652 (1993).
50. Lee, C. T., Yang, W. T. & Parr, R. G. Development of the colle-salvetti correlation-energy formula into a functional of the electron-density. *Phys. Rev. B* **37**, 785–789 (1988).
51. Hay, P. J. & Wadt, W. R. Abinitio effective core potentials for molecular calculations - potentials for k to au including the outermost core orbitals. *J. Chem. Phys.* **82**, 299–310 (1985).
52. Hay, P. J. & Wadt, W. R. Abinitio effective core potentials for molecular calculations - potentials for the transition-metal atoms Sc to Hg. *J. Chem. Phys.* **82**, 270–283 (1985).
53. Wadt, W. R. & Hay, P. J. Abinitio effective core potentials for molecular calculations - potentials for main group elements Na to Bi. *J. Chem. Phys.* **82**, 284–298 (1985).

Acknowledgments

The authors acknowledge the financial support from the National Key Scientific Program-Nanoscience and Nanotechnology (2011CB933700) and the National Natural Science Foundation of China (Grant Nos. 61106012, 61102013, and 21073197). X.-J.H. acknowledges the CAS Institute of Physical Science, University of Science and Technology of China (2012FXCX008), for financial support.

Author contributions

X.J.H. conceived and designed the experiments. Z.G. carried out all the experiments and calculations. Z.G. and X.J.H. co-wrote the paper. Z.G.L., X.Z.Y., K.S.Z., X.C. and J.H.L. contributed data analysis and interpretation equally. All the authors viewed the manuscript.

Additional information

Supplementary information accompanies this paper at http://www.nature.com/scientificreports

Competing financial interests: The authors declare no competing financial interests.

How to cite this article: Guo, Z. *et al.* A molecular-gap device for specific determination of mercury ions. *Sci. Rep.* **3**, 3115; DOI:10.1038/srep03115 (2013).